

Parallel measurements of reaction kinetics using ultra-low volumes

Etienne Fradet,^a Paul Abbyad,^{b,c} Marten Vos,^c and Charles N. Baroud^a

Contents

1	Mixing experiment	2
2	Reaction-diffusion model	3
3	Fitting procedures	5
4	Comparison of the simulations and the experiments	8
5	Channel height measurements	9
6	Movies	9

^a *Laboratoire d'Hydrodynamique (LadHyX) and Department of Mechanics, Ecole Polytechnique, CNRS, 91128, Palaiseau, France. E-mail: baroud@ladhyx.polytechnique.fr*

^b *Department of Chemistry & Biochemistry, Santa Clara University, 500 El Camino Real, Santa Clara, California, USA*

^c *Laboratoire d'Optique et Biosciences (LOB), Ecole Polytechnique, INSERM U696, CNRS, 91128 Palaiseau, France.*

1 Mixing experiment

In order to assess the diffusive transport of the reagents when two droplets are merged in our reaction chamber, we fused two water droplets, one of which being dyed as shown on Fig. 1a. During the coalescence phase, the droplet interface undergoes strong deformations which yields a strong flow inside the droplet but no significant mixing. As a result, a sharp front separating the pure water from the dyed water forms as shown on Fig. 1b. After some hundreds of ms, the droplet interface has relaxed to its final shape and the initial front of dye is smoothed out by diffusion.

Measuring the dye concentration along the daughter droplet yields an error function of width σ . We thus followed σ over time which increases as $t^{1/2}$ as shown on Fig. 1f. In addition, fitting the measurements of $\sigma(t)$ with $y = \sqrt{4D_B t}$ yields $D_B = 0.77 \times 10^9 \text{ m}^2/\text{s}$ which agrees well with other measurements of this diffusion coefficient.

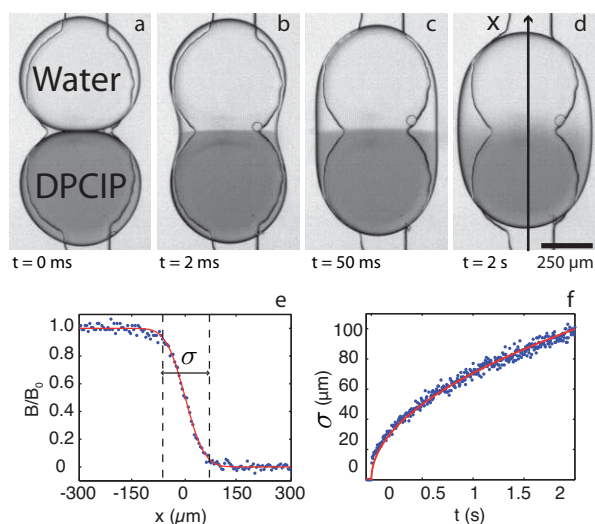


Figure 1: (a)-(d) Snapshots at different time points of the fusion of two equally sized droplets, one containing the dark blue DCPIP at 6 mM, the other containing buffer only. A sharp front forms just after the fusion start. Once the interface has reached its final shape, the dye diffuses freely across the daughter droplet. (e) Measure of the dye concentration along the daughter droplet at $t = 1 \text{ s}$. The dye profile is an error function of width σ . (f) Evolution of σ over time. The solid line is the best fit of the experimental measurements with $y = \sqrt{4D_B t}$ which yields $D_B = 0.77 \times 10^9 \text{ m}^2/\text{s}$.

2 Reaction-diffusion model

Chemical system We consider two reagents, namely L-ascorbic acid (denoted A) and DCPIP (denoted B), placed in two different droplets as shown on Fig. 2a. Once the droplets are merged, A and B diffuse toward each other with given diffusion constants D_A and D_B , and react at a rate k . The reaction is bimolecular and assumed to follow a second order reaction rate $R = kAB$ where $A(x, t)$ and $B(x, t)$ are the local concentrations of A and B. The reaction scheme reads as:



where A and B are the reagents and C is the product of the reaction.

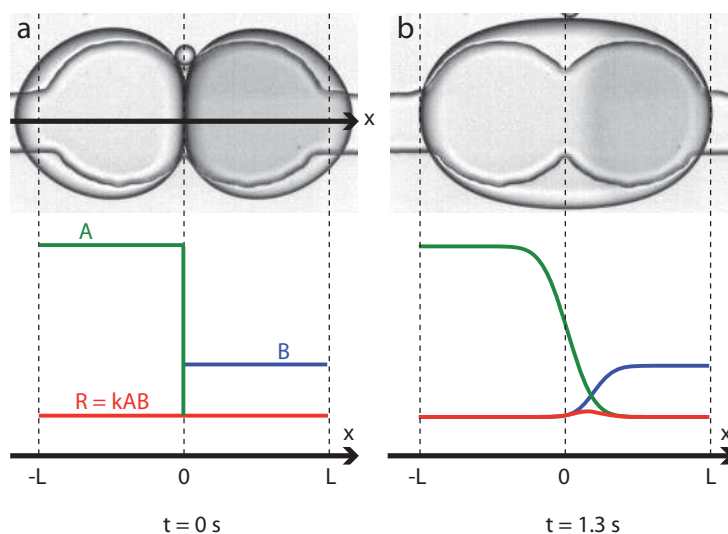


Figure 2: The experiment consists in merging two droplets of diameter $L \approx 500 \mu\text{m}$, each droplet containing a different reagent. Here, L-ascorbic acid at 100 mM is placed on the left hand side and DCPIP at 0.6 mM is placed on the right hand side. (a) Initial conditions: Reagents A and B are perfectly separated and modeled as two touching Heaviside functions. (b) Profiles of reagents A and B at $t = 1.3 \text{ s}$ given by the reaction-diffusion model.

Initial conditions A straight separation line between the A rich region and the B rich region forms during the droplet coalescence. We thus model the initial profiles of A and B by two touching Heaviside functions H while C is initially zero:

$$A = A_0 H(x \leq 0), \quad B = B_0 H(x \geq 0), \quad C = 0 \quad (2)$$

Reaction-diffusion model This initial straight separation line then diffuses and propagates across the daughter droplet as A and B react. This is shown on Fig. 2b. We thus model the diffusive transport along the daughter droplet only and label this direction with the x coordinate as

defined on Fig. 2a. Conservation laws for A, B and C then read as 1D diffusion equations coupled by the reaction rate $R = kAB$:

$$\frac{\partial A}{\partial t} = D_A \frac{\partial^2 A}{\partial x^2} - kAB, \quad (3)$$

$$\frac{\partial B}{\partial t} = D_B \frac{\partial^2 B}{\partial x^2} - kAB, \quad (4)$$

$$\frac{\partial C}{\partial t} = D_C \frac{\partial^2 C}{\partial x^2} + kAB, \quad (5)$$

Boundary conditions Finally, we impose no-flux boundary conditions at the edges of the daughter droplet as droplets are not permeable:

$$\frac{\partial A}{\partial x} = \frac{\partial B}{\partial x} = \frac{\partial C}{\partial x} = 0 \quad \text{at } x = \pm L \quad (6)$$

Numerical resolution The problem set by the equations (2)-(6) is solve numerically using the MATLAB routine `pdepe` with the physical variables shown in Table 1. The only unknown is the rate constant k which is treated as a fitting parameters.

L (μm)	D_A ($\times 10^9$ m^2/s)	D_B ($\times 10^9$ m^2/s)	D_C ($\times 10^9$ m^2/s)	A_0 (mM)	B_0 (mM)
500	0.87	0.77	0.87	10 to 100	0.6

Table 1: Values of the parameters used to solve the RD model (2)-(6). D_B was measured in droplets as shown in section 1. D_A was estimated from D_B with the relationships $D_A = (M_b/M_a)^{1/3} \cdot D_B$ and $D_C = (M_b/M_c)^{1/3} \cdot D_B$ where M_a , M_b and M_c are the molar weights of A, B and C.

3 Fitting procedures

Profiles of B were measured in the daughter droplet $x \in [-L, L]$ and on a given time window $t \in [0, t_{end}]$. In order to test our model, we fitted experimental profiles of B with numerical solutions of the RD model using two different fitting procedures:

Local fit Fit on the local profiles of B, denoted $B(x, t)$, for $x \in [-L, L]$ and $t \in [0, t_{end}]$,

Integrated fit Fit on the mean value of B, denoted $\overline{B}(t)$, over time for $t \in [0, t_{end}]$.

The mean value of B was defined according to the daughter droplet size L by:

$$\overline{B}(t) = \frac{1}{2L} \int_{-L}^L B(x, t) dx \quad (7)$$

Each fitting procedure reads as follows:

1. Definition of the error:

$$\text{error} = \frac{\|B^{\text{exp}} - B^{\text{sim}}\|}{\|B^{\text{exp}}\|} \quad \text{or} \quad \text{error} = \frac{\|\overline{B}^{\text{exp}} - \overline{B}^{\text{sim}}\|}{\|\overline{B}^{\text{exp}}\|} \quad (8)$$

2. Compute the error for increasing values of k on a given time window t_{end}
3. Repeat the previous step for increasing values of the time window t_{end}

For each values of the time window t_{end} , plots of the error against guess values of the observed rate k_{obs} are thus obtained as shown on Fig. 3 and 4. For small time windows $t_{end} < 1$ s, plots are flat which means that no value of k_{obs} is selected by the RD model. For larger time window $t_{end} > 1$ s, plots take a valley shape of increasing steepness with increasing time window t_{end} . In addition, the value of k_{obs} where the valley is minimal is constant which shows that the RD model selects only one value of k_{obs} . On the other hand, the value of the error in the bottom of the valley first decreases as t_{end} is increased, but increases again for $t_{end} > 4$ s in the local fitting procedure as shown on Fig. 3. As a result, we fixed $t_{end} = 4$ s and took the best fit value of k_{obs} in that case as a measure of the actual observed rate. In addition, confidence intervals can be extracted from these plots by measuring the steepness of the valley as shown on Fig. 5. Measurements of the observed rate k_{obs} and corresponding confidence interval are shown in table 2. Finally, values of the rate constant k using the two different fitting procedures are compared to the value obtained using a stopped-flow in table 3.

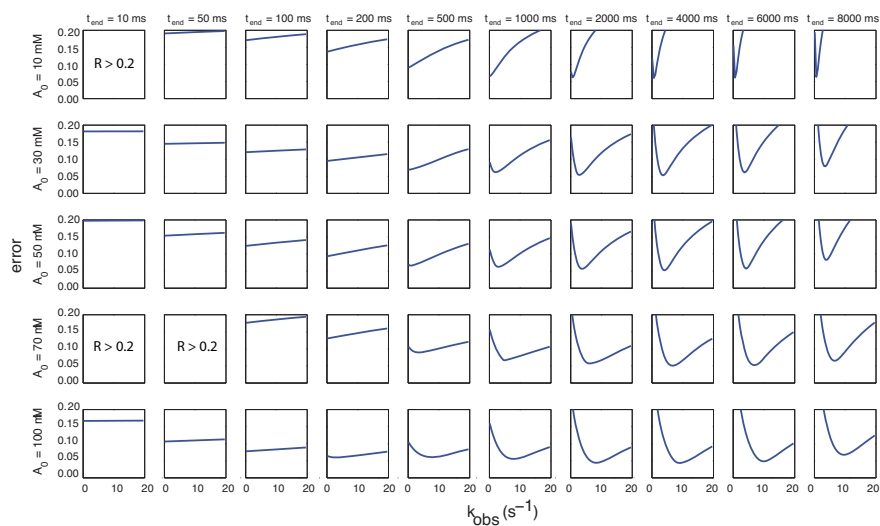


Figure 3: Error of the local fitting procedures against the fitting parameter $k_{obs} = kA_0$ for different time window t_{end} .

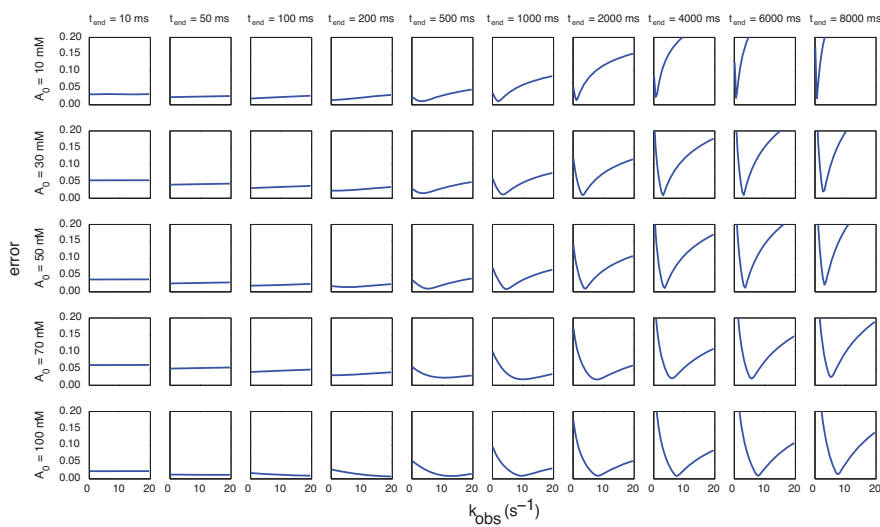


Figure 4: Residuals of the glocal fitting procedures against the fitting parameter $k_{obs} = kA_0$ for different time window t_{end} .

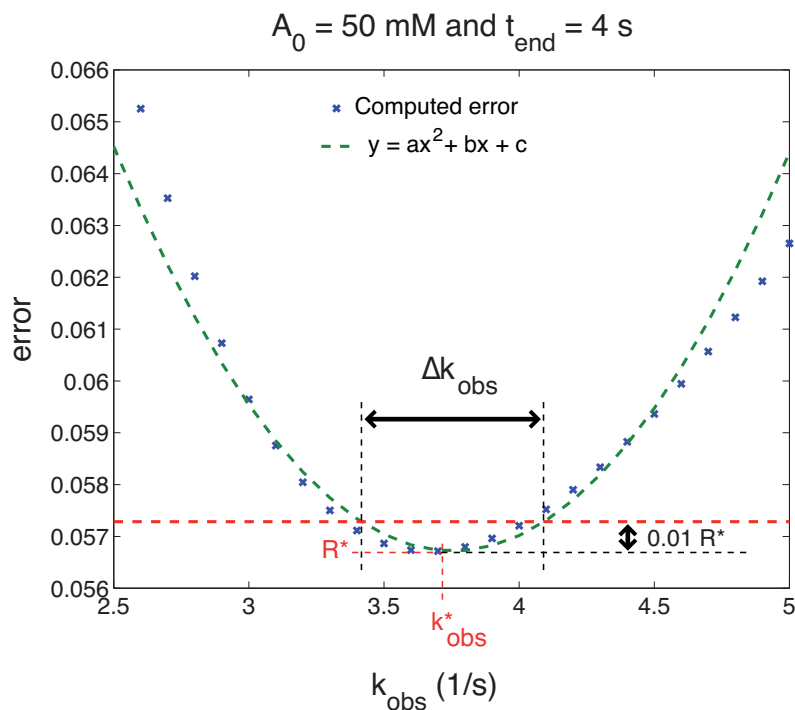


Figure 5: Confidence interval definition for $A_0=50 \text{ mM}$ and $t_{\text{end}}=4 \text{ s}$. The best fit values is denoted $[k_{\text{obs}}^* R^*]$. The confidence interval Δk_{obs} is defined as the interval around k_{obs}^* in which the residuals is between its minimum R^* and $1.01 R^*$. This is a measure of the steepness of the valley.

RD model	A_0 (mM)	10	30	50	70	100
local	k_{obs}^* (1/s)	0.71	2.90	3.80	6.30	8.30
local	Δk_{obs} (1/s)	0.26	0.57	0.67	1.20	1.23
integrated	k_{obs}^* (1/s)	0.93	3.13	3.61	6.03	7.63
integrated	Δk_{obs} (1/s)	0.11	0.12	0.16	0.40	0.24

Table 2: Confidence intervals measured for two different fitting procedures with $t_{\text{end}} = 4 \text{ s}$. Each plot on Fig. 3 and 4 has a minimum $[k_{\text{obs}}^* R^*]$. Confidence intervals are defined here as the interval Δk_{obs} in which the residuals varies in $[0.99R^* \ 1.01R^*]$.

	Stopped-flow	RD local	Local integrated
k (1/M/s)	86.7	82.8	79.7
Residuals	0.9863	0.994	0.983

Table 3: Values the rate k extracted by measuring the slope of $k_{\text{obs}} = kA_0$ against A_0 by three different methods. The mean value and the standard deviation of these measurements yields $k = 83.1 \pm 3.5 \text{ 1/M/s}$. These measurements are within 8 % from each other.

4 Comparison of the simulations and the experiments

We present here the comparison between our measurements in droplets and the best profiles obtained with our model. Fig. 6 shows space-time diagrams obtained by juxtaposing DCPIP profiles along the daughter droplet at successive time points. The first row presents experimental space-time diagrams for increasing initial concentration in L-ascorbic acid. The second row presents the corresponding simulations with the best fit value of the observed rate k_{obs} . Fig. 7 shows the mean amount of DCIP along the daughter droplet for different time points. Experimental and numerical curves are superposed. The different plots corresponds to different values of the initial concentration in L-ascorbic acid.

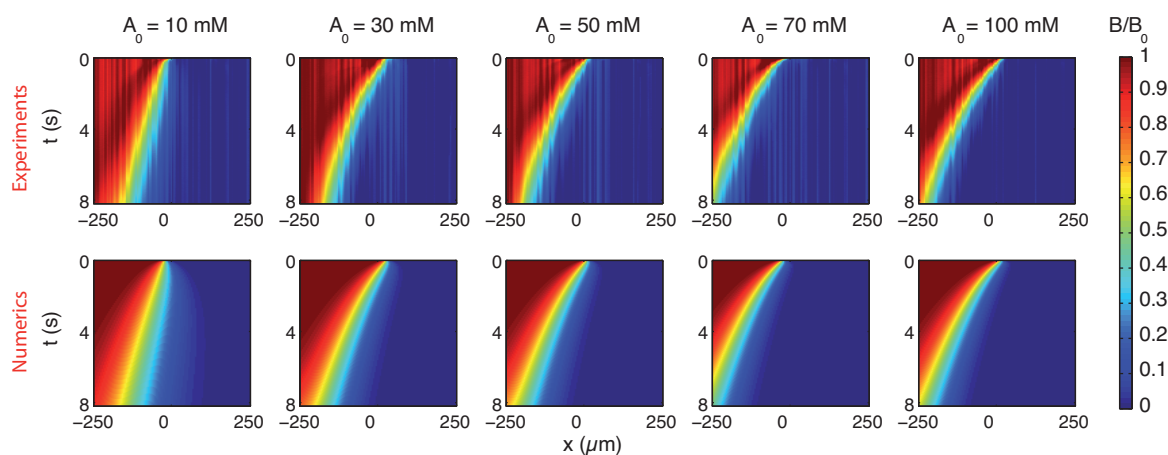


Figure 6: Experimental and simulated space-time diagrams for different initial concentration of L-ascorbic acid A_0 . Simulations were done with the best fit value of k_{obs} .

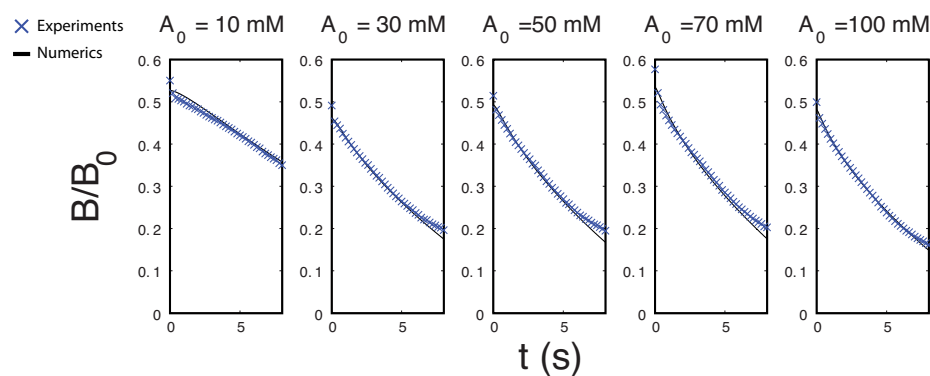


Figure 7: Superposition of the experimental and the simulated mean value of B obtained for different initial concentration of L-ascorbic acid A_0 . Simulations were done with the best fit value of k_{obs} .

5 Channel height measurements

Finally we present measurements of the channel molds used for this paper on Fig. 8. This measurements have been done with a Zygo NewView 7100 profilometer.

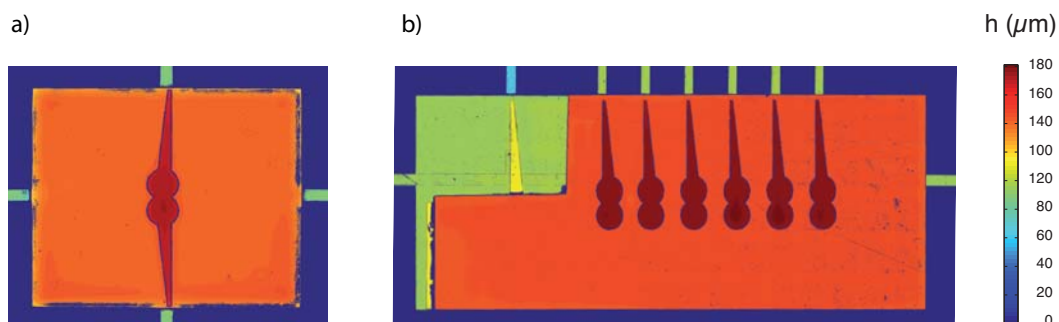


Figure 8: Channel height measurements of the molds obtained by soft lithography. (a) Single trap reaction chamber. (b) Multiple traps reaction chamber.

6 Movies

Three movies are attached to the manuscript:

Movie S1: Channel operation of the reaction chamber with DCPIP/L-ascorbic.

Movie S2: Fusion of two droplets in the reaction chamber, one containing DCPIP at 6 mM, the other is pure water. This experiment is detailed in the section 1 of the supplementary informations.

Movie S3: Filling procedure of the parallelized chip. Each inlet is connected to a different input to allow different conditions to be tested on chip.